ACS APPLIED MATERIALS & INTERFACES

Research Article

www.acsami.org

Intracellular Cascade FRET for Temperature Imaging of Living Cells with Polymeric Ratiometric Fluorescent Thermometers

Xianglong Hu,*[,†,‡] Yang Li,[‡] Tao Liu,[‡] Guoying Zhang,*[,‡] and Shiyong Liu*[,‡]

[†]MOE Key Laboratory of Laser Life Science and Institute of Laser Life Science, College of Biophotonics, South China Normal University, Guangzhou 510631, China

[‡]CAS Key Laboratory of Soft Matter Chemistry, Hefei National Laboratory for Physical Sciences at the Microscale, iChem (Collaborative Innovation Center of Chemistry for Energy Materials), Department of Polymer Science and Engineering, University of Science and Technology of China, Hefei, Anhui 230026, China

Supporting Information

ABSTRACT: Intracellular temperature plays a prominent role in cellular functions and biochemical activities inside living cells, but effective intracellular temperature sensing and imaging is still in its infancy. Herein, thermoresponsive double hydrophilic block copolymers (DHBCs)-based fluorescent thermometers were fabricated to investigate their application in intracellular temperature imaging. Blue-emitting coumarin monomer, CMA, green-emitting 7-nitro-2,1,3-benzoxadiazole (NBD) monomer, NBDAE, and red-emitting rhodamine B monomer, RhBEA, were copolymerized separately with *N*-isopropylacrylamide (NIPAM) to afford dye-labeled PEG-*b*-P(NIPAM-*co*-CMA), PEG-*b*-P(NIPAM-*co*-NBDAE), and PEG-*b*-P(NIPAM-*co*-RhBEA). Because of the favorable fluorescence resonance energy transfer (FRET) potentials between CMA and NBDAE, NBDAE and RhBEA, as well as the slight tendency between CMA and RhBEA fluorophore pairs, three polymeric thermometers based on traditional one-step FRET were fabricated by facile mixing two of these three fluorescent DHBCs, whereas exhibiting limited advantages. Thus, two-step cascade FRET among three polymeric fluorophores was further interrogated, in which NBD acted as a bridging dye by transferring energy from CMA to RhBEA. Through the delicate optimization of the molar contents of three polymeric components, a ~8.4-fold ratio change occurred in the temperature range of 20−44 °C, and the detection sensitivity improved significantly, reached as low as ~0.4 °C, which definitely outperformed other one-step FRET thermometers in the intracellular temperature imaging of living cells. To our knowledge, this work represents the first example of polymeric ratiometric thermometer employing thermoresponsive polymer-based cascade FRET mechanism.

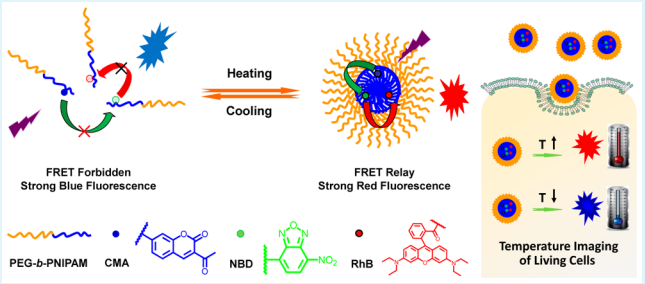

KEYWORDS: *intracellular temperature imaging, cascade FRET, PNIPAM, polymeric ratiometric thermometers, thermoresponsive DHBCs*

INTRODUCTION

Temperture is a significant parameter in a broad range of biological activities, especially in biological reactions within living cells.[1−4] In addition, various abnormal medical phenonmena ranging from inflammation to cancer cell growth are often accompanied by temperature increase. Unfortunately, in situ and noninvasive determination and real-time monitoring of intracellular temperature accurately at microscale or nanoscale is still a poorly resolved problem.[5−9] In this context, fluorescent thermometers are attracting more and more attention due to their intrinsic advantages such as high spatial resolution and functional independence of the medium.[10−13] A great variety of fluorescent thermometers employing different fluorescence techniques (e.g., fluorescence intensity and lifetime)[14−19] and different fluorophores (such as small organic dyes,[20] fluorescent proteins,[21,22] upconversion nanoparticles,[23] quantum dots,[24] metal complexes,[25,26] and GFP-based thermosensors[27]) have been developed. Among these, small molecule-based sensors usually suffer from major limitations such as poor water solubility, low structural stability, and difficulty in further functionalization. Alternatively, polymeric sensors with flexible structural design and optimal properties have been increasingly utilized as a novel approach.[28−35]

Thermoresponsive hydrophilic poly(*N*-isopropylacrylamide), PNIPAM, bearing polarity or viscosity sensitive organic dyes have been investigated intensively as fluorescent thermometers in recent years. Typically, Uchiyama and co-workers developed a series of PNIPAM-based fluorescent thermometers by introducing 4-*N*,*N*-dimethylamino-7-*N*,*N*-dimethylaminosulfonyl-2-1-3-benzoxadiazole (DBD-NMe_2) or its derivatives into PNIPAM.[15] After that, they fabricated an elegant example of fluorescence lifetime-based fluorescent thermometer and

Received: May 9, 2015
Accepted: June 26, 2015
Published: June 26, 2015

DOI: 10.1021/acsami.5b04025
ACS Appl. Mater. Interfaces 2015, 7, 15551−15560

mapped the intracellular temperature variations among different organelles based on fluorescence lifetime imaging microscopy for the first time.[18] The nucleus temeprature was demonstrated to be slightly higher than that of cytoplasm and the temperature gap was varied depending on the stages of cell cycles.

It should be noted that fluorescent thermometers based on the fluorescence intensity changes at certain wavelengths are more prevalent and easier to access compared with that of fluorescence lifetime. However, the fluorescence intensity at a single wavelength can be affected by many parameters (e.g., dye concentration, photobleaching).[36−38] For further insight into the role of temperature in the intracellular events, ratiometric fluorescent thermometers that can be achieved by various strategies are preferred due to their potential advantages.[39] Moreover, fluorescence resonance energy transfer (FRET) is very powerful in analyte detection and sensing.[40] For the ratiometric fluorescent thermometers based on thermo-induced FRET mechanism, pyrene and its quencher fullerene-labeled PNIPAM polymeric temperature sensor has been developed.[41] Additionally, the integration of a thermosensitive dye and an insensitive reference physically embeded within a polymeric hydrophobic core was also employed to probe the temperature of living cells,[42] but the incovalent nature of fluorophores within nanoparticles would inevitably face the problem of dye diffusion and leakage as well as limited controllability that would restrict their further applications.

Besides conventional one-step FRET between two fluorophores, cascade FRET between three or more fluorophores is receiving more and more attention, especially in the investigation of complex biological macromolecular interactions.[43] A much longer FRET radius can be realized based on cascade FRET, thus making it more effective for the exploration of long-range molecular interactions, enzymatic conformational change, and many biological activities concerning three or more biomacromolecular interactions, in which the spatial distances between active moieties are often longer than traditional FRET radius.[44−56] Typically, Watrob and co-workers investigated the two-step FRET theoretically and experimetnally, demonstrating that two-step cascade FRET is more suitable in a broad range of research area than one-step FRET such as long-range energy transfer.[57]

Inspired by the exciting characteristics of the cascade FRET, we envisage the integration of a two-step cascade FRET process with the design of a polymeric ratiometric fluorescent thermometer (Scheme 1). Well-defined thermoresponsive DHBCs, blue-emitting PEG-*b*-P(NIPAM-*co*-CMA), green-emitting PEG-*b*-P(NIPAM-*co*-NBDAE), and red-emitting PEG-*b*-P(NIPAM-*co*-RhBEA) were fabricated via reversible addition−fragmentation chain transfer (RAFT) polymerization in the presence of NIPAM, fluorescent monomers, and PEG-based RAFT agent, respectively (Scheme S1 of the Supporting Information). Three types of one-step FRET thermometers were achieved facilely by mixing two of these three kinds of fluorescent DHBCs, but the performance was not satisfactory. However, facile integration of three different DHBCs into one system afforded a novel polymeric ratiometric thermometer, in which NBD acted as a FRET bridge by transferring the emitted fluorescence energy of CMA to RhBEA, exhibiting improved performance both in aqueous solution and in intracellular temperature imaging of living cells.

Scheme 1. (a) Fabrication of Polymeric Ratiometric Fluorescent Thermometers from Thermoresponsive Double Hydrophilic Block Copolymers (DHBCs), Blue-Emitting CMA- Labeled PEG-*b*-P(NIPAM-*co*-CMA), Green-Emitting NBDAE-Labeled PEG-*b*-P(NIPAM-*co*-NBDAE), and Red-Emitting RhBEA-Labeled PEG-*b*-P(NIPAM-*co*-RhBEA) via the NBD-Mediated Two-Step Cascade FRET Process; (b) Schematic Illustration for the Intracellular Temperature Imaging and Temperature Readout of Living Cells upon Cellular Internalization of the Cascade FRET Thermometer

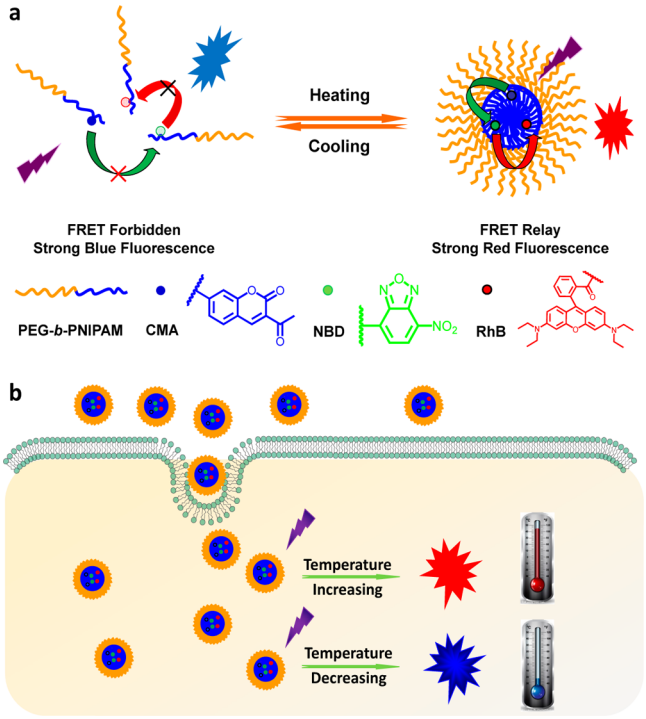

EXPERIMENTAL SECTION

Materials. *N*-Isopropylacrylamide (NIPAM) (97%, Tokyo Kasei Kagyo Co.) was purified by recrystallization from a mixture of benzene and *n*-hexane (1/3, v/v). 2,2′-Azobis(2-methylpropionitrile) (AIBN) was obtained from Acros chemicals and recrystallized from 95% ethanol. 1,4-Dioxane, tetrahydrofuran (THF), and other reagents were purchased from Sinopharm Chemical Reagent Co. Ltd. and used as received. Water was deionized with a Milli-Q SP reagent water system (Millipore) to a specific resistivity of 18.4 MΩ cm. PEG-based macroRAFT agent,[58] coumarin-based monomer (CMA),[59] NBD-based monomer (NBDAE),[14,60] and rhodamine B-based monomer (RhBEA)[61] were synthesized according to literature procedures.

Sample Synthesis. Typical RAFT polymerization routes employed for the preparation of thermoresponsive fluorophore-labeled DHBCs,[62,63] PEG-*b*-P(NIPAM-*co*-CMA), PEG-*b*-P(NIPAM-*co*-NBDAE), and PEG-*b*-P(NIPAM-*co*-RhBEA) are shown in Scheme S1 of the Supporting Information.

Synthesis of PEG-b-P(NIPAM-co-CMA), PEG-b-P(NIPAM-co-NBDAE), and PEG-b-P(NIPAM-co-RhBEA) DHBCs. Typical procedures for the synthesis of DHBCs are as follows. PEG-based macroRAFT agent (0.40 g, 0.08 mmol), NIPAM (1.09 g, 9.6 mmol), CMA (25 mg, 0.08 mmol), AIBN (1.3 mg, 0.008 mmol), and 1,4-dioxane (5 mL) were added into a reaction tube. The mixture was carefully degassed by three freeze−thaw cycles, and then sealed under vacuum. After stirring at 70 °C for 2 h, the reaction tube was opened and diluted with 5 mL THF. The mixture was then precipitated into an excess of cooled ethyl ether. The above dissolution−precipitation cycle was repeated for three times. The final product was dried in a vacuum oven overnight at room temperature to afford PEG-*b*-P(NIPAM-*co*-CMA) diblock

DOI: 10.1021/acsami.5b04025
ACS Appl. Mater. Interfaces 2015, 7, 15551−15560

Table 1. Molecular Parameters and Dynamic Laser Light Scattering (LLS) Characterization and LCST Determination of Polymers Used in This Work

samples	$M_{n,GPC}$ (kDa)[a]	M_w/M_n[a]	$M_{n,NMR}$ (kDa)[b]	R_h (nm)[c]	PDI[c]	LCST (°C)[d]
PEG_{113} macroRAFT agent	5.0	1.07				
PEG_{113}-*b*-P(NIPAM-*co*-CMA)$_{97}$	15.4	1.13	16.0	32.5	0.16	34.0
PEG_{113}-*b*-P(NIPAM-*co*-NBDAE)$_{95}$	15.8	1.11	15.7	26.7	0.09	35.6
PEG_{113}-*b*-P(NIPAM-*co*-RhBEA)$_{89}$	14.9	1.16	15.1	25.6	0.10	35.8
mixed micellar dispersion[e]				26.8	0.13	

[a]Determined by GPC using DMF as the eluent (1.0 mL/min). [b]Calculated from ^{1}H NMR results. [c]Determined by dynamic LLS at a copolymer concentration of 1 mg/mL at 50 °C. [d]Determined by temperature dependence of optical transmittance at 700 nm for 2.0 g/L DHBCs. Temperature at which 10% transmittance drop was determined to be LCST. [e]Mixed micellar dispersion fabricated from PEG-*b*-P(NIPAM-*co*-CMA), PEG-*b*-P(NIPAM-*co*-NBDAE), and PEG-*b*-P(NIPAM-*co*-RhBEA).

copolymers as a white powder. PEG-*b*-P(NIPAM-*co*-CMA) was then treated with an excess of AIBN (130 mg, 0.8 mmol) in 1,4-dioxane (5 mL) under nitrogen at 70 °C for 2 h. The mixture was then precipitated into an excess of *n*-hexane. The above dissolution-precipitation cycle was repeated for three times. After drying in a vacuum oven overnight, PEG-*b*-P(NIPAM-*co*-CMA) was obtained as a white powder (0.76 g; yield, 50.2%). The molecular weight and molecular weight distribution were determined by GPC using DMF as the eluent, revealing an M_n of 15.4 kDa and M_w/M_n of 1.13 (Table 1). The degree of polymerization, DP, of PNIPAM block was determined to be 97 by ^{1}H NMR analysis in $CDCl_3$. CMA content in P(NIPAM-*co*-CMA) block was determined to be ~0.57 mol % (corresponding to ~0.55 CMA per polymer chain) based on UV−vis spectroscopy in water by using CMA monomer as the calibration standard at room temperature. Thus, the polymer was denoted as PEG_{113}-*b*-P(NIPAM$_{0.9943}$-*co*-CMA$_{0.0057}$)$_{97}$ and shortened as PEG-*b*-P(NIPAM-*co*-CMA) in subsequent sections. With similar procedures, two other polymers were also synthesized (Table 1): PEG_{113}-*b*-P(NIPAM-*co*-NBDAE)$_{95}$ (M_n = 15.8 kDa, M_w/M_n = 1.11; NBDAE content: ~0.63 NBDAE per polymer chain) and PEG_{113}-*b*-P(NIPAM-*co*-RhBEA)$_{89}$ (M_n = 14.9 kDa, M_w/M_n = 1.16; RhBEA content: ~0.60 RhBEA per polymer chain), which have been shortened as PEG-*b*-P(NIPAM-*co*-NBDAE) and PEG-*b*-P(NIPAM-*co*-RhBEA) in the following sections, respectively.

In Vitro Cytotoxicity Assay. HepG2 cells were employed for in vitro cytotoxicity evaluation via the MTT assay. HepG2 cells were first cultured in Dulbecco's modified Eagle medium (DMEM) supplemented with 10% fetal bovine serum (FBS), penicillin (100 units/mL), and streptomycin (100 μg/mL) at 37 °C in a CO_2/air (5:95) incubator for 2 days. For cytotoxicity assay, HepG2 cells were seeded in a 96-well plate at an initial density of ca. 5000 cells/well in 100 μL of complete DMEM medium. After incubating for 24 h, DMEM was replaced with fresh medium, and the cells were treated with polymer aqueous solution at varying concentrations. The treated cells were incubated in a humidified environment with 5% CO_2 at 37 °C for 48 h. The MTT reagent (in 20 μL PBS, 5 mg/mL) was added to each well. The cells were further incubated for 4 h at 37 °C. The medium in each well was then removed and replaced with 150 μL DMSO. The plate was gently agitated for 15 min before the absorbance at 570 nm was recorded by a microplate reader (Thermo Fisher). Each experiment condition was done in quadruple and the data are shown as the mean value plus a standard deviation (±SD).

Cell Culture and in Vitro Fluorescence Imaging. HepG2 cells were cultured in Dulbecco's modified Eagle medium (DMEM) supplemented with 10% fetal bovine serum (FBS), penicillin (100 units/mL), and streptomycin (100 μg/mL) at 37 °C in a CO_2/air (5:95) incubator for 2 days. All the intracellular temperature imaging experiments were carried out with similar procedures. Typically, HepG2 cells were treated with the mixed aqueous solution of 0.35 g/L PEG-*b*-P(NIPAM-*co*-CMA) and 0.1 g/L PEG-*b*-P(NIPAM-*co*-NBDAE) for 40 min at 37 °C in a CO_2/air (5:95) incubator and then rinsed with PBS (3 × 1 mL) and replaced with new PBS for further imaging experiments. The cell imaging experiments at different temperatures were conducted from high temperature to low temperature using inverted Leica TCS SP5 confocal microscope equipped with a heating stage. The calibration curve used for determining intracellular temperature was obtained by calculating the fluorescence intensity ratio of 0.35 g/L PEG-*b*-P(NIPAM-*co*-CMA) and 0.1 g/L PEG-*b*-P(NIPAM-*co*-NBDAE) in cell extract at varying temperatures based on literature procedures.[18] The fluorescence emission was harvested at 410−450 nm for the blue channel, 510−550 nm for green channel, and 565−605 nm for red channel. The excitation was chosen as 405 nm for CMA-NBDAE, CMA-RhBEA, and CMA-NBDAE-RhBEA pairs and chosen as 488 nm for NBDAE-RhBEA pair. For the experiment of external chemical stimuli-induced intracellular temperature change, HepG2 cells were first stained with PEG-*b*-P(NIPAM-*co*-CMA) (0.14 g/L, 4.8 × 10^{-6} M), PEG-*b*-P(NIPAM-*co*-NBDAE) (0.28 g/L, 1.1 × 10^{-5} M), and PEG-*b*-P(NIPAM-*co*-RhBEA) (0.04 g/L, 1.6 × 10^{-6} M) for 40 min at 37 °C and then the culture DMEM was replaced with PBS before further incubating for another 30 min. The HepG2 cells were imaged at 37 °C before and after replacing PBS with DMEM containing 100 mM glucose.

Characterization. All ^{1}H nuclear magnetic resonance (NMR) spectra were recorded on a Bruker AV300 NMR spectrometer (resonance frequency of 300 MHz for ^{1}H NMR) operated in the Fourier transform mode. $CDCl_3$ was used as the solvent. Molecular weights and molecular weight distributions were determined by gel permeation chromatography (GPC) equipped with Waters 1515 pump and Waters 2414 differential refractive index detector (set at 30 °C), employing a series of two linear Styragel columns (HR2 and HR4) at an oven temperature of 45 °C. The eluent was DMF at a flow rate of 1.0 mL/min. A series of low polydispersity polystyrene standards were employed for calibration. All UV−vis spectra were acquired on a Unico UV/vis 2802PCS spectrophotometer. The transmittance of the aqueous solutions was acquired at a wavelength of 700 nm. A thermostatically controlled cuvette was employed, and the heating rate was 0.2 °C min^{-1}. Dynamic laser light scattering (LLS) measurements were conducted on a commercial spectrometer (ALV/DLS/SLS-5022F) equipped with a multi-tau digital time correlator (ALV5000) and a cylindrical 22 mW UNIPHASE He−Ne laser (λ_0 = 632.8 nm) as the light source. Scattered light was collected at a fixed angle of 90° for duration of ~5 min. Distribution averages and particle size distributions were computed using cumulants analysis and CONTIN routines. All data were averaged over three measurements. Fluorescence spectra were recorded on F-4600 spectrofluorometer (Hitachi). The temperature of the water-jacketed cell holder was controlled by a programmable circulation bath. The slit widths were set at 5 nm for both excitation and emission.

RESULTS AND DISCUSSION

Synthesis and Thermoresponsive Micellization of Dye-Labeled DHBCs. Well-defined thermoresponsive DHBCs bearing fluorophores were synthesized via reversible addition-fragmentation chain transfer (RAFT) polymerization (Scheme S1 of the Supporting Information). Typically, CMA-labeled PEG-*b*-P(NIPAM-*co*-CMA) was fabricated employing RAFT polymerization in the presence of NIPAM, CMA, and

DOI: 10.1021/acsami.5b04025
ACS Appl. Mater. Interfaces 2015, 7, 15551−15560

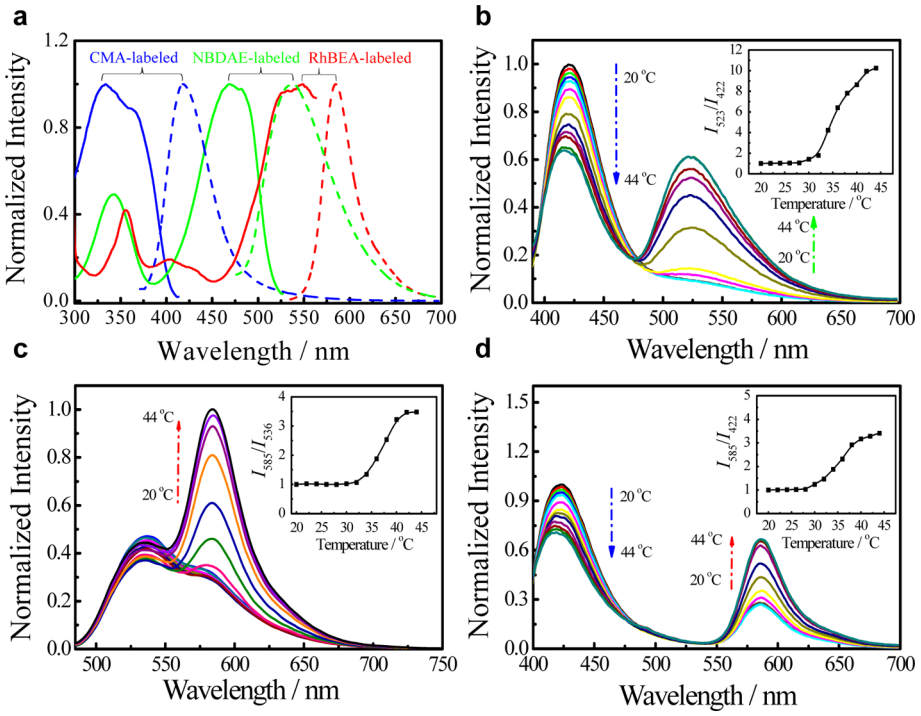

Figure 1. (a) Fluorescence excitation (solid line) and emission spectra (dotted line) recorded for the aqueous solution of CMA-labeled PEG-*b*-P(NIPAM-*co*-CMA), NBDAE-labeled PEG-*b*-P(NIPAM-*co*-NBDAE), and RhBEA-labeled PEG-*b*-P(NIPAM-*co*-RhBEA). Fluorescence emission spectra and normalized intensity ratio (insets) recorded in the range of 20−44 °C for three types of polymeric aqueous solution: (b) PEG-*b*-P(NIPAM-*co*-CMA) (0.35 g/L, [CMA] = 1.2×10^{-5} M) and PEG-*b*-P(NIPAM-*co*-NBDAE) (0.1 g/L, [NBDAE] = 4.0×10^{-6} M) (λ_{ex} = 365 nm; I_{523}/I_{422}). (c) PEG-*b*-P(NIPAM-*co*-NBDAE) (0.1 g/L, [NBDAE] = 4.0×10^{-6} M) and PEG-*b*-P(NIPAM-*co*-RhBEA) (0.1 g/L, [RhBEA] = 4.0×10^{-6} M) (λ_{ex} = 470 nm; I_{585}/I_{536}). (d) PEG-*b*-P(NIPAM-*co*-CMA) (0.14 g/L, 4.8×10^{-6} M), PEG-*b*-P(NIPAM-*co*-NBDAE) (0.28 g/L, 1.1×10^{-5} M), and PEG-*b*-P(NIPAM-*co*-RhBEA) (0.04 g/L, 1.6×10^{-6} M) (λ_{ex} = 365 nm; I_{585}/I_{422}) (slit widths: Ex. 5 nm, Em. 5 nm).

PEG-based RAFT agent in 1,4-dioxane at 70 °C, revealing an M_n of 15.4 kDa and M_w/M_n of 1.13 based on GPC analysis (Table 1). The degree of polymerization, DP, of PNIPAM block was determined to be ~97 by ^{1}H NMR analysis in $CDCl_3$. CMA content in P(NIPAM-*co*-CMA) block was determined to be ~0.57 mol % (corresponding to ~0.55 CMA per chain) with UV−vis spectroscopy. Thus, the polymer was denoted as PEG_{113}-*b*-$P(NIPAM_{0.9943}$-*co*-$CMA_{0.0057})_{97}$ and shortened as PEG-*b*-P(NIPAM-*co*-CMA) in the following sections. Combined with similar procedures, PEG_{113}-*b*-P(NIPAM-*co*-NBDAE)$_{95}$ (M_n = 15.8 kDa, M_w/M_n = 1.11; NBDAE content: ~0.63 NBDAE per chain) and PEG_{113}-*b*-P(NIPAM-*co*-RhBEA)$_{89}$ (M_n = 14.9 kDa, M_w/M_n = 1.16; RhBEA content: ~0.60 RhBEA per chain) were synthesized (Table 1) and shortened as PEG-*b*-P(NIPAM-*co*-NBDAE) and PEG-*b*-P(NIPAM-*co*-RhBEA), respectively.

In view of the thermosensitivity of PNIPAM, the thermo-induced micellization behavior of these DHBCs was demonstrated at first. The hydrodynamic radius of micelles formed at elevated temperature for PEG-*b*-P(NIPAM-*co*-CMA), PEG-*b*-P(NIPAM-*co*-NBDAE), and PEG-*b*-P(NIPAM-*co*-RhBEA) were determined to be ~32.5, 26.7, and 25.6 nm by dynamic laser light scattering (LLS), respectively. Then the lower critical solution temperatures (LCSTs) of thermoresponsive PEG-*b*-P(NIPAM-*co*-CMA), PEG-*b*-P(NIPAM-*co*-NBDAE), and PEG-*b*-P(NIPAM-*co*-RhBEA) were demonstrated to be ~34.0, 35.6, and 35.8 °C, respectively. In addition, the size and distribution for mixed micellar dispersion fabricated from three diblock coplymers was also analyzed, exhibiting comparable results compared with that of single micellar dispersion (Table 1).

Insight into the Performance of Polymeric Ratiometric Fluorescent Thermometers. FRET has been widely recognized as a versatile tool for the study of biomacromolecular structures, intracellular molecular interactions, fluorescence assays, and nucleic acid analysis.[64−67] As shown in Figure 1a, the fluorescence emission spectra of PEG-*b*-P(NIPAM-*co*-CMA) and PEG-*b*-P(NIPAM-*co*-NBDAE) overlapped with the excitation spectra of PEG-*b*-P(NIPAM-*co*-NBDAE) and PEG-*b*-P(NIPAM-*co*-RhBEA) respectively, which is prerequisite for FRET. However, a poor overlap between the emission spectrum of PEG-*b*-P(NIPAM-*co*-CMA) and the excitation spectrum of PEG-*b*-P(NIPAM-*co*-RhBEA) was observed, implying limited FRET efficiency between them.

Then, the temperature-dependent fluorescence variation for three dye-labeled DHBCs was explored separately. The fluorescence intensity of CMA-labeled PEG-*b*-P(NIPAM-*co*-CMA) and RhBEA-labeled PEG-*b*-P(NIPAM-*co*-RhBEA) dropped slightly upon heating, exhibiting approximate 44% and 32% intensity decrease in the temperature range 20−44 °C (Figure S1a−d of the Supporting Information). On the contrary, almost one fold fluorescence enhancement was observed for NBDAE-labeled PEG-*b*-P(NIPAM-*co*-NBDAE) presumably due to the polarity sensitivity of NBD derivatives (Figure S1e,f of the Supporting Information).[68] Overall, no dramatic fluorescence change was observed for these three DHBCs upon heating.

In an effort to fabricate polymeric ratiometric fluorescent thermometers, one-step and two-step cascade FRET systems, which were constructed by mixing two or three dye-labeled DHBCs together, were investigated and compared in detail. As

DOI: 10.1021/acsami.5b04025
ACS Appl. Mater. Interfaces 2015, 7, 15551−15560

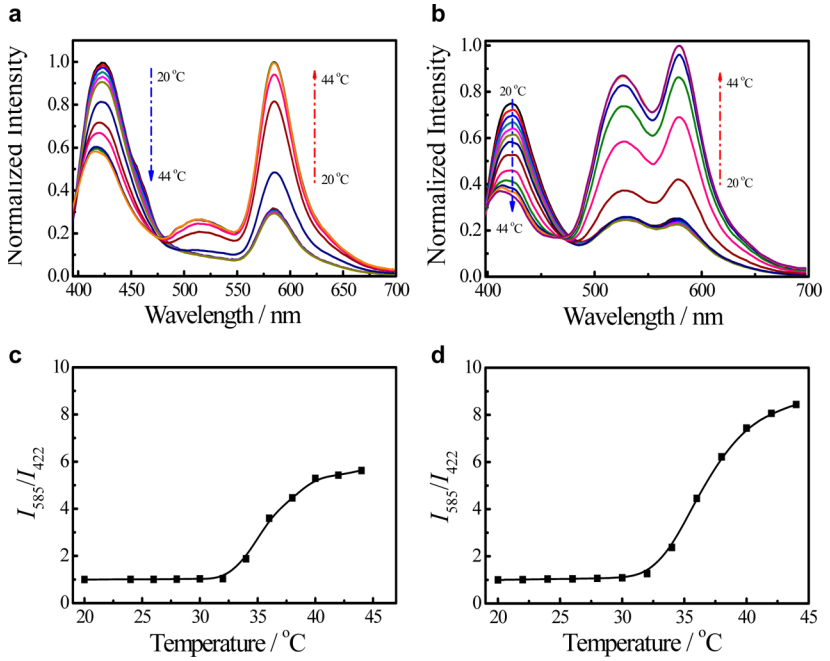

Figure 2. Fluorescence emission spectra recorded for the aqueous solution of (a) PEG-*b*-P(NIPAM-*co*-CMA) (0.35 g/L, [CMA] = 1.2×10^{-5} M), PEG-*b*-P(NIPAM-*co*-NBDAE) (0.1 g/L, [NBDAE] = 4.0×10^{-6} M), and PEG-*b*-P(NIPAM-*co*-RhBEA) (0.1 g/L, [RhBEA] = 4.0×10^{-6} M), and (b) PEG-*b*-P(NIPAM-*co*-CMA) (0.14 g/L, 4.8×10^{-6} M), PEG-*b*-P(NIPAM-*co*-NBDAE) (0.28 g/L, 1.1×10^{-5} M), and PEG-*b*-P(NIPAM-*co*-RhBEA) (0.04 g/L, 1.6×10^{-6} M) in the range of 20−44 °C. (c and d) Normalized intensity ratio changes (I_{585}/I_{422}) recorded for that in panels a and b, respectively (λ_{ex} = 365 nm; slit widths: Ex. 5 nm, Em. 5 nm).

shown in Figure 1b, the ratiometric fluorescent thermometer based on blue-emitting PEG-*b*-P(NIPAM-*co*-CMA) and green-emitting PEG-*b*-P(NIPAM-*co*-NBDAE) was explored at first. A strong fluorescence emission peak at 422 nm could be observed while the fluorescence emission at 523 nm was almost negligible at 20 °C. Upon gradually increasing the temperature, the fluorescence intensity at 422 nm decreased constantly accompanied by a slight blue shift. Concomitantly, the fluorescence intensity at 523 nm increased substantially, especially in the temperature range of 32−40 °C. Accordingly, approximately 10.3-fold intensity ratio change (I_{523}/I_{422}) was obtained in a broad temperature range of 20−44 °C mainly in temperature range of 31−44 °C (Figure 1b inset).

In addition, the one-step FRET ratiometric thermometer fabricated from green-emitting PEG-*b*-P(NIPAM-*co*-NBDAE) and red-emitting PEG-*b*-P(NIPAM-*co*-RhBEA) also exhibited a fluorescence ratio change yet with different characteristics (Figure 1c). Strong green fluorescence at 536 nm and an almost indiscernible red fluorescence peak at 585 nm were observed at lower temperature. Upon heating, the two peaks dropped a little at first, and then recovered to original level for the green emission and increased dramatically for the red emission. The slight change of fluorescence emission at 536 was possibly due to the presumable combination of hydrophobic fluorescence enhancement and FRET-induced fluorescence decrease of NBDAE donor in the range of 20−44 °C. Overall, a ~3.5-fold ratiometric change (I_{585}/I_{536}) was obtained primarily in the range of 33−40 °C (Figure 1c inset). Additionally, one-step FRET between CMA-labeled PEG-*b*-P(NIPAM-*co*-CMA) and RhBEA-labeled PEG-*b*-P(NIPAM-*co*-RhBEA) was also explored despite the poor FRET tendency disclosed previously (Figure 1d). Corresponding to the decrease of fluorescence intensity at 422 nm, the fluorescence intensity at 585 nm exhibited ~2-fold enhancement, and the intensity ratio (I_{585}/I_{422}) only changed ~3.4-fold in the temperature range of 20−44 °C.

It should be mentioned that apart from the number of folds, the fluorescence signal changed in a broad temperature range. The sensitive variation of signals in a narrow temperature range especially around biological temperature is of equal importance for the acquisition of a deeper insight into the role of temperature in intracellular events.[10] After all, the temperature variations in biological systems often occur in a narrow temperature range. The sensitivity at a certain temperature can be roughly evaluated by the differential function derived from the signal change-temperature curve. The differential function revealed that the fluorescence signal of the ratiometric system based on CMA-NBDAE changed slowly in a broader range and the highest slope is ~0.1 K^{-1} at 31.2 °C (Figure S2a of the Supporting Information). The highest slopes of the differential function for the one-step FRET system based on NBDAE-RhBEA and CMA-RhBEA were determined to be 0.2 K^{-1} at 37.6 °C and 0.07 K^{-1} at 35.9 °C, respectively (Figure S2b,c of the Supporting Information).

Recently, cascade FRET among three or more fluorophores has been increasingly focused owing to its outstanding characteristics in many areas, ranging from long-range molecular interactions to biomacromolecular conformational changes.[44−57] Inpired by this, we introduced two-step cascade FRET into the design of ratiometric fluorescent thermometers based on the desirable FRET efficiency in two pairs of fluorephores, i.e., PEG-*b*-P(NIPAM-*co*-CMA) and PEG-*b*-P(NIPAM-*co*-NBDAE) as well as that between PEG-*b*-P(NIPAM-*co*-NBDAE) and PEG-*b*-P(NIPAM-*co*-RhBEA). Thermo-induced micellization of dye-labeled PNIPAM chains decreased the spatial distance of three fluorogens in the mixed micellar core, which is the basic requirement for FRET (Scheme 1), thus possible two-step energy transfer from CMA

DOI: 10.1021/acsami.5b04025
ACS Appl. Mater. Interfaces 2015, 7, 15551−15560

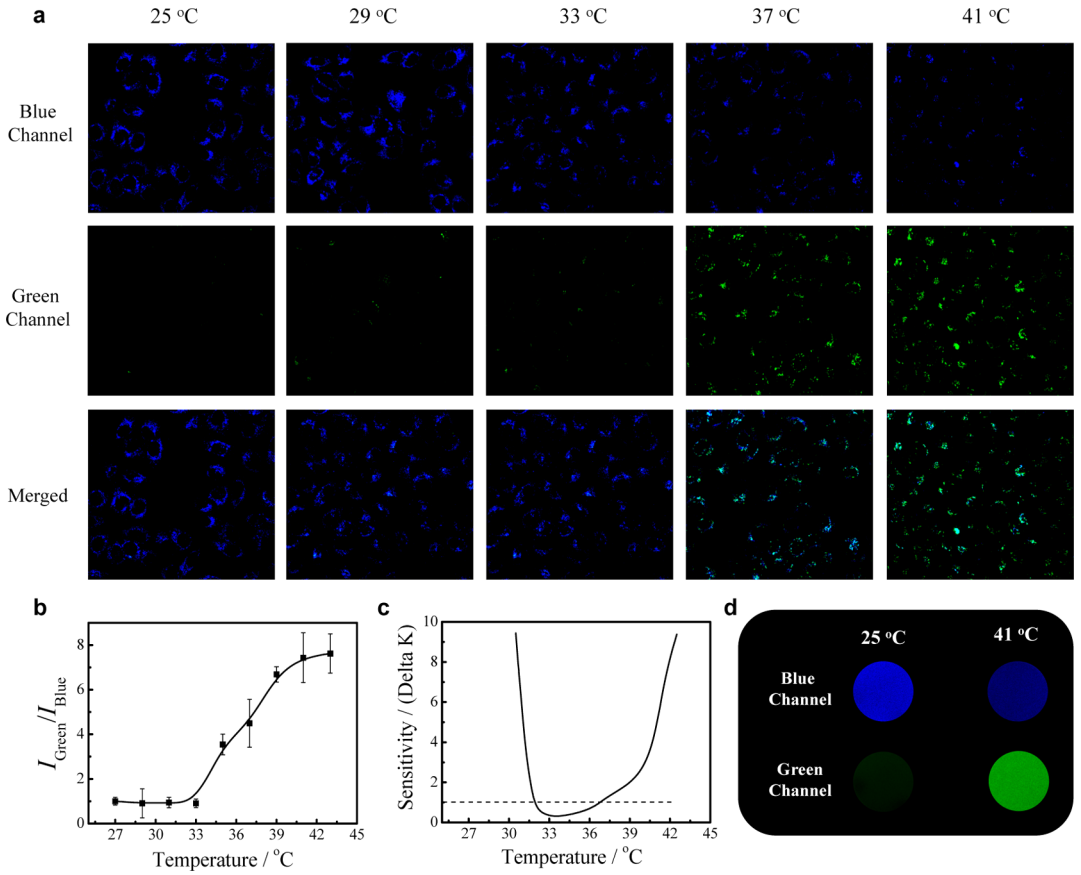

Figure 3. (a) Confocal microscopy fluorescence images, (b) normalized intensity ratio (I_{green}/I_{blue}) changes, and (c) detection sensitivity recorded by confocal microscopy (λ_{ex} = 405 nm) for live HepG2 cells in the temperature range of 25−42 °C after incubating at 37 °C for 40 min with the aqueous solution of PEG-*b*-P(NIPAM-*co*-CMA) (0.35 g/L, [CMA] = 1.2 × 10^{-5} M) and PEG-*b*-P(NIPAM-*co*-NBDAE) (0.1 g/L, [NBDAE] = 4.0 × 10^{-6} M). (d) Fluorescence images recorded for above aqueous solution at 25 and 41 °C, respectively.

to NBD, and then from NBD to RhBEA was expected to exist in the mixed micellar core fabricated from three dye-labeled DHBCs. First, a certain amount of PEG-*b*-P(NIPAM-*co*-NBDAE) was added into the ratiometric thermometer system of PEG-*b*-P(NIPAM-*co*-CMA) and PEG-*b*-P(NIPAM-*co*-RhBEA). As shown in Figure 2a, a dramatic fluorescence decrease at 422 nm and substantial fluorescence enhancement at 585 nm was observed upon heating. However, the fluorescence enhancement of NBDAE was limited in comparison with the results in Figure 1b. Together with much more remarkable enhancement of RhBEA emission at 585 nm, there should be a two-step FRET occurred, namely a cascade FRET process first from CMA to NBDAE and then from NBDAE to RhBEA existed exactly; meanwhile, there was also a possible one-step FRET process from CMA to RhBEA, thus a ∼5.6-fold total intensity ratio (I_{585}/I_{422}) change was obtained in the temperature range of 20−44 °C mainly in the narrow range of 32−40 °C (Figure 2c). Differential analysis revealed the highest slope was ∼0.19 K^{-1} at 35.1 °C, which is comparable with that of the ratiometric system based on NBDAE-RhBEA but apparent larger than that of the ratiometric system based on CMA-NBDAE and CMA-RhBEA (Figure S2d vs Figure S2a,c of the Supporting Information). The delicate modulation of blending ratios among three polymeric fluorophores was further examined, then a ratiometric fluorescent thermometer derived from a two-step cascade FRET process was fabricated with improved performance, in which a ∼8.4-fold intensity ratio (I_{585}/I_{422}) change was revealed in the temperature range of 20−44 °C, mainly in the range of 32−44 °C (Figure 2b,d). Differential analysis suggested that the highest slope was about 0.3 K^{-1} at 35.9 °C, which was much better than previous one-step FRET thermometers (Figure S2e of the Supporting Information).

Moreover, polymeric fluorescent thermometers internalized via endocytosis would mostly be exposed to intracellular pH gradients and fluctuations.[69−71] Thus, the fluorescence stability of CMA, NBDAE, and RhBEA-labeled DHBCs against different pH values was interrogated independently, exhibiting excellent pH insensitivity to promise the accuracy of temperature sensing (Figure S3a−c of the Supporting Information). In addition, the reversibility experiments cycled over ten times between different temperatures revealed that the ratiometric fluorescent thermometers were suitable for repeated temperature imaging reversibly (Figure S4a−e of the Supporting Information). Finally, in vitro cytotoxicity against HepG2 cells upon incubation with PEG-*b*-P(NIPAM-*co*-CMA), PEG-*b*-P(NIPAM-*co*-NBDAE), and PEG-*b*-P(NIPAM-*co*-RhBEA) revealed that these DHBCs were relatively nontoxic to HepG2 cells at high concentrations up to 1 g/L (Figure S5 of the Supporting Information).

Intracellular Temperature Imaging with Polymeric Ratiometric Thermometers. In view of the importance of temperature on the biological events within living cells, intracellular temperature imaging was conducted. In comparison, the intracellular temperature sensing and mapping with one-step FRET thermometers based on CMA-NBDAE,

DOI: 10.1021/acsami.5b04025
ACS Appl. Mater. Interfaces 2015, 7, 15551−15560

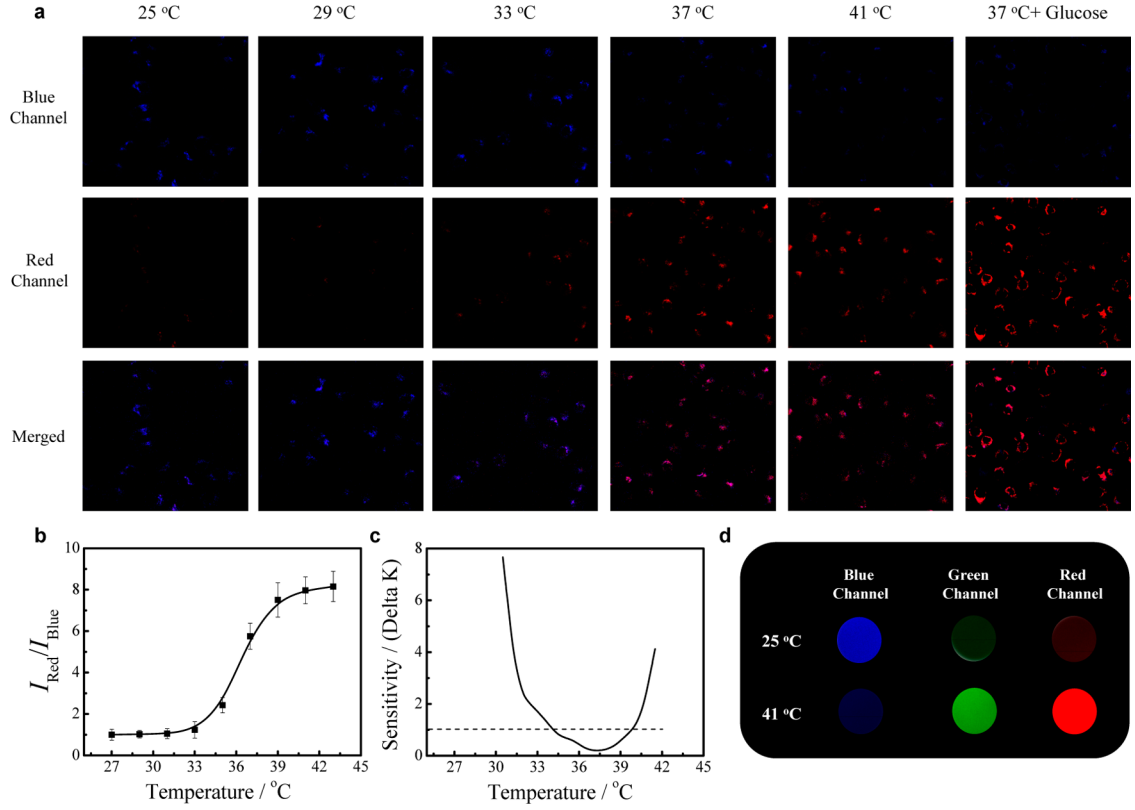

Figure 4. (a) Confocal microscopy fluorescence images, (b) normalized intensity ratio (I_{red}/I_{blue}) changes, and (c) detection sensitivity recorded by confocal microscopy (λ_{ex} = 405 nm) for live HepG2 cells in the temperature range of 25−42 °C after incubating at 37 °C for 40 min with the aqueous solution of PEG-*b*-P(NIPAM-*co*-CMA) (0.14 g/L, [CMA] = 4.8 × 10^{-6} M), PEG-*b*-P(NIPAM-*co*-NBDAE) (0.28 g/L, [NBDAE] = 1.1 × 10^{-5} M), and PEG-*b*-P(NIPAM-*co*-RhBEA) (0.04 g/L, [RhBEA] = 1.6 × 10^{-6} M). For the glucose treated sample, the cells were imaged after incubating with DMEM containing 100 mM glucose at 37 °C for 30 min. (d) Fluorescence images recorded for above aqueous solution at 25 and 41 °C, respectively.

NBDAE-RhBEA, CMA-RhBEA polymeric fluorescent pairs and two-step cascade FRET thermometers from CMA-NBDAE-RhBEA were investigated parallelly in subsequent sections. As shown in Figure 3a, a strong blue emission of living cells was observed whereas the green emission was almost indiscernible in the temperature below 33 °C for the ratiometric fluorescent thermometer based on PEG-*b*-P(NIPAM-*co*-CMA) and PEG-*b*-P(NIPAM-*co*-NBDAE). However, at temperature above 33 °C, the green emission increased substantially and the blue emission exhibited fluorescence decrease to some extent. The temperature calibration curve was performed based on confocal microscopy, and the temperature detection sensitivity was also calculated (Figure 3b,c).[16] In the range of 32−36.7 °C, the temperature detection sensitivity was determined to be less than 1 °C and the highest sensitivity was ∼0.32 °C at 33.3 °C. Meanwhile, fluorescence imaging for the mixed aqueous solution of PEG-*b*-P(NIPAM-*co*-CMA) and PEG-*b*-P-(NIPAM-*co*-NBDAE) was also performed at 25 and 41 °C, which agreed well with aforementioned results (Figure 3d).

Nonetheless, the intracellular performance of ratiometric fluorescent thermometer based on one-step FRET between PEG-*b*-P(NIPAM-*co*-NBDAE) and PEG-*b*-P(NIPAM-*co*-RhBEA) was compromised, compared with that in aqueous solution. Discernable intracellular fluorescence variation was observed for the red channel, but not for the green channel, in the temperature range of 25−41 °C (Figure S6a,b,d of the Supporting Information). In the meantime, the detection sensitivity was suboptimal, higher than 1 °C in the whole experimental temperature range (Figure S6c of the Supporting Information). Similarly, the one-step FRET fluorescent thermometer based on PEG-*b*-P(NIPAM-*co*-CMA) and PEG-*b*-P(NIPAM-*co*-RhBEA) was also examined in the same profile (Figure S7a−d of the Supporting Information). The red fluorescence enhancement can be observed in a relatively broader temperature range, and a relatively better sensitivity (∼0.62 °C) around 35.5 °C was displayed.

Conversely, the two-step cascade FRET-based polymeric fluorescent thermometer fabricated from PEG-*b*-P(NIPAM-*co*-CMA), PEG-*b*-P(NIPAM-*co*-NBDAE), and PEG-*b*-P(NIPAM-*co*-RhBEA) with an optimized blending ratio behaved much better than foregoing one-step FRET thermometers in the intracellular temperature mapping. As shown in Figure 4a, strong blue emission and minimal red emission can be observed at temperature below 33 °C. However, the red emission increased dramatically accompanied by the sharp decrease of blue emission at higher temperature. In combination with the analysis of calibration curve, the two-step cascade-FRET thermometer showed much more satisfactory detection sensitivity, which was determined to be lower than 1 °C in a broad temperature range of 34.2−40.5 °C, and the best sensitivity reached ∼0.40 °C at 37 °C (Figure 4b,c). In view of its practical application, external stimuli-induced change of intracellular temperature was further probed. As shown in the last row of Figure 4a, the cells exhibited moderate blue emission and red emission after starvation in PBS for 30 min at 37 °C. After PBS was replaced with fresh DMEM containing

DOI: 10.1021/acsami.5b04025
ACS Appl. Mater. Interfaces 2015, 7, 15551−15560

100 mM glucose, a prominent enhancement of red emission and decrease of blue emission could be observed, suggesting heat generation within living cells upon glucose treatment.[18] Quantitative analysis revealed that the temperature of the cells increased approximately to 37.6 °C (±0.17), which was in good agreement with previous results.[18] Likewise, the fluorescence images for the mixed aqueous solution of three DHBCs with optimized blending ratio coincided with the aforementioned results of intracellular temperature imaging (Figure 4d).

CONCLUSIONS

In summary, a series of polymeric ratiometric thermometers based on one-step FRET and two-step cascade FRET mechanisms were fabricated successfully from thermoresponsive DHBCs, CMA-labeled PEG-*b*-P(NIPAM-*co*-CMA), NBDAE-labeled PEG-*b*-P(NIPAM-*co*-NBDAE), and RhBEA-labeled PEG-*b*-P(NIPAM-*co*-RhBEA). The intracellular temperature imaging of living cells by these ratiometric thermometers was explored in parallel. Compared with other one-step FRET thermometers, improved performance was demonstrated by the two-step cascade FRET based thermometer, in which NBD acted as a FRET mediator by transferring the emission energy from CMA to RhBEA, exhibiting a ∼8.4-fold ratio change in the temperature range of 20−44 °C. Furthermore, a detection sensitivity of less than 1 °C was observed in a broad temperature range of 34.2−40.5 °C, and the highest sensitivity reached as low as ∼0.4 °C at 37 °C. More importantly, the intracellular temperature fluctuations after starvation and a glucose feed were manifested by our two-step FRET system. This work discloses the noteworthy capability for polymeric thermometers based on the cascade FRET process, and their sensing potency for subcellular temperature distribution and evolution is under endeavor. Current intracellular cascade FRET thermometers would probably assist the comprehension of intracellular temperature-related reactions and lesions, such as signal transduction, cellular pathogenesis of cancer and inflammation, and thereby aid future exploration in the medical field.

ASSOCIATED CONTENT

Supporting Information

Synthetic routes, spectroscopic analysis, cell toxicity, and intracellular temperature imaging of living cells. The Supporting Information is available free of charge on the ACS Publications website at DOI: 10.1021/acsami.5b04025.

AUTHOR INFORMATION

Corresponding Authors

*X. Hu. E-mail: xlhu@scnu.edu.cn.
*G. Zhang. E-mail: gyzhang@ustc.edu.cn.
*S. Liu. E-mail: sliu@ustc.edu.cn.

Notes

The authors declare no competing financial interest.

ACKNOWLEDGMENTS

The financial support from the National Natural Scientific Foundation of China (NNSFC) Projects (21274137, 51273190, 51033005, 51473153, and 51403042) and Specialized Research Fund for the Doctoral Program of Higher Education (SRFDP, 20123402130010) and the Natural Science Foundation of Guangdong Province, China (2014A030310310) is gratefully acknowledged.

REFERENCES

(1) Seymour, R. S. Biophysics and Physiology of Temperature Regulation in Thermogenic Flowers. *Biosci. Rep.* **2001**, *21*, 223−236.
(2) Warner, D. A.; Shine, R. The Adaptive Significance of Temperature-Dependent Sex Determination in a Reptile. *Nature* **2008**, *451*, 566−568.
(3) Bahat, A.; Tur-Kaspa, I.; Gakamsky, A.; Giojalas, L. C.; Breitbart, H.; Eisenbach, M. Thermotaxis of Mammalian Sperm Cells: A Potential Navigation Mechanism in the Female Genital Tract. *Nat. Med.* **2003**, *9*, 149−150.
(4) Wilkinson, D. M. Treelines, Climate and Temperature Regulation in Plants - a Wider Context for Korner's Views on the Importance of Plant Architecture. *Plant Ecol. Divers.* **2009**, *2*, 1−4.
(5) Wang, X. D.; Wolfbeis, O. S.; Meier, R. J. Luminescent Probes and Sensors for Temperature. *Chem. Soc. Rev.* **2013**, *42*, 7834−7869.
(6) Cui, Y. J.; Song, R. J.; Yu, J. C.; Liu, M.; Wang, Z. Q.; Wu, C. D.; Yang, Y.; Wang, Z. Y.; Chen, B. L.; Qian, G. D. Dual-Emitting MOF superset of Dye Composite for Ratiometric Temperature Sensing. *Adv. Mater.* **2015**, *27*, 1420−1425.
(7) McLaurin, E. J.; Bradshaw, L. R.; Gamelin, D. R. Dual-Emitting Nanoscale Temperature Sensors. *Chem. Mater.* **2013**, *25*, 1283−1292.
(8) Jaque, D.; Vetrone, F. Luminescence Nanothermometry. *Nanoscale* **2012**, *4*, 4301−4326.
(9) Kucsko, G.; Maurer, P. C.; Yao, N. Y.; Kubo, M.; Noh, H. J.; Lo, P. K.; Park, H.; Lukin, M. D. Nanometre-Scale Thermometry in a Living Cell. *Nature* **2013**, *500*, 54−58.
(10) Pietsch, C.; Schubert, U. S.; Hoogenboom, R. Aqueous Polymeric Sensors Based on Temperature-Induced Polymer Phase Transitions and Solvatochromic Dyes. *Chem. Commun.* **2011**, *47*, 8750−8765.
(11) Wang, S. P.; Westcott, S.; Chen, W. Nanoparticle Luminescence Thermometry. *J. Phys. Chem. B* **2002**, *106*, 11203−11209.
(12) Brites, C. D. S.; Lima, P. P.; Silva, N. J. O.; Millan, A.; Amaral, V. S.; Palacio, F.; Carlos, L. D. Lanthanide-Based Luminescent Molecular Thermometers. *New J. Chem.* **2011**, *35*, 1177−1183.
(13) Sakaguchi, R.; Kiyonaka, S.; Mori, Y. Fluorescent Sensors Reveal Subcellular Thermal Changes. *Curr. Opin. Biotechnol.* **2015**, *31*, 57−64.
(14) Uchiyama, S.; Matsumura, Y.; de Silva, A. P.; Iwai, K. Fluorescent Molecular Thermometers Based on Polymers Showing Temperature-Induced Phase Transitions and Labeled with Polarity-Responsive Benzofurazans. *Anal. Chem.* **2003**, *75*, 5926−5935.
(15) Iwai, K.; Matsumura, Y.; Uchiyama, S.; de Silva, A. P. Development of Fluorescent Microgel Thermometers Based on Thermo Responsive Polymers and Their Modulation of Sensitivity Range. *J. Mater. Chem.* **2005**, *15*, 2796−2800.
(16) Gota, C.; Okabe, K.; Funatsu, T.; Harada, Y.; Uchiyama, S. Hydrophilic Fluorescent Nanogel Thermometer for Intracellular Thermometry. *J. Am. Chem. Soc.* **2009**, *131*, 2766−2767.
(17) Uchiyama, S.; Kawai, N.; de Silva, A. P.; Iwai, K. Fluorescent Polymeric AND Logic Gate with Temperature and pH as Inputs. *J. Am. Chem. Soc.* **2004**, *126*, 3032−3033.
(18) Okabe, K.; Inada, N.; Gota, C.; Harada, Y.; Funatsu, T.; Uchiyama, S. Intracellular Temperature Mapping with a Fluorescent Polymeric Thermometer and Fluorescence Lifetime Imaging Microscopy. *Nat. Commun.* **2012**, *3*, 705.
(19) Balducci, A.; Wen, Y.; Zhang, Y.; Helfer, B. M.; Hitchens, T. K.; Meng, W. S.; Wesa, A. K.; Janjic, J. M. A Novel Probe for the Non-Invasive Detection of Tumor-Associated Inflammation. *Oncoimmunology* **2013**, *2*, e23034.
(20) Nagai, A.; Yoshii, R.; Otsuka, T.; Kokado, K.; Chujo, Y. BODIPY-Based Chain Transfer Agent: Reversibly Thermoswitchable Luminescent Gold Nanoparticle Stabilized by BODIPY-Terminated Water-Soluble Polymer. *Langmuir* **2010**, *26*, 15644−15649.
(21) Wong, F. H. C.; Banks, D. S.; Abu-Arish, A.; Fradin, C. A Molecular Thermometer Based on Fluorescent Protein Blinking. *J. Am. Chem. Soc.* **2007**, *129*, 10302−10303.
(22) Donner, J. S.; Thompson, S. A.; Kreuzer, M. P.; Baffou, G.; Quidant, R. Mapping Intracellular Temperature Using Green Fluorescent Protein. *Nano Lett.* **2012**, *12*, 2107−2111.

DOI: 10.1021/acsami.5b04025
ACS Appl. Mater. Interfaces 2015, 7, 15551−15560

(23) Fischer, L. H.; Harms, G. S.; Wolfbeis, O. S. Upconverting Nanoparticles for Nanoscale Thermometry. *Angew. Chem., Int. Ed.* **2011**, *50*, 4546−4551.
(24) Albers, A. E.; Chan, E. M.; McBride, P. M.; Ajo-Franklin, C. M.; Cohen, B. E.; Helms, B. A. Dual-Emitting Quantum Dot/Quantum Rod-Based Nanothermometers with Enhanced Response and Sensitivity in Live Cells. *J. Am. Chem. Soc.* **2012**, *134*, 9565−9568.
(25) Wang, X. D.; Song, X. H.; He, C. Y.; Yang, C. J.; Chen, G. N.; Chen, X. Preparation of Reversible Colorimetric Temperature Nanosensors and Their Application in Quantitative Two-Dimensional Thermo-Imaging. *Anal. Chem.* **2011**, *83*, 2434−2437.
(26) Peng, H. S.; Stich, M. I. J.; Yu, J. B.; Sun, L. N.; Fischer, L. H.; Wolfbeis, O. S. Luminescent Europium(III) Nanoparticles for Sensing and Imaging of Temperature in the Physiological Range. *Adv. Mater.* **2010**, *22*, 716−719.
(27) Kiyonaka, S.; Kajimoto, T.; Sakaguchi, R.; Shinmi, D.; Omatsu-Kanbe, M.; Matsuura, H.; Imamura, H.; Yoshizaki, T.; Hamachi, I.; Morii, T.; Mori, Y. Genetically Encoded Fluorescent Thermosensors Visualize Subcellular Thermoregulation in Living Cells. *Nat. Methods* **2013**, *10*, 1232−1238.
(28) Li, Y. W.; Zhang, W. B.; Janoski, J. E.; Li, X. P.; Dong, X. H.; Wesdemiotis, C.; Quirk, R. P.; Cheng, S. Z. D. Anionic Synthesis of Mono- and Heterotelechelic Polystyrenes via Thiol-Ene "Click" Chemistry and Hydrosilylation. *Macromolecules* **2011**, *44*, 3328−3337.
(29) Li, K.; Liu, B. Polymer-Encapsulated Organic Nanoparticles for Fluorescence and Photoacoustic Imaging. *Chem. Soc. Rev.* **2014**, *43*, 6570−6597.
(30) Rochat, S.; Swager, T. M. Conjugated Amplifying Polymers for Optical Sensing Applications. *ACS Appl. Mater. Interfaces* **2013**, *5*, 4488−4502.
(31) Hu, X. L.; Liu, G. H.; Li, Y.; Wang, X. R.; Liu, S. Y. Cell-Penetrating Hyperbranched Polyprodrug Amphiphiles for Synergistic Reductive Milieu-Triggered Drug Release and Enhanced Magnetic Resonance Signals. *J. Am. Chem. Soc.* **2015**, *137*, 362−368.
(32) Li, C. H.; Wu, T.; Hong, C. Y.; Zhang, G. Q.; Liu, S. Y. A General Strategy To Construct Fluorogenic Probes from Charge-Generation Polymers (CGPs) and AIE-Active Fluorogens through Triggered Complexation. *Angew. Chem., Int. Ed.* **2012**, *51*, 455−459.
(33) Liu, T.; Zhang, Y. F.; Liu, S. Y. Drug and Plasmid DNA Co-delivery Nanocarriers Based on ABC-Type Polypeptide Hybrid Miktoarm Star Copolymers. *Chin. J. Polym. Sci.* **2013**, *31*, 924−937.
(34) Wan, X. J.; Wang, D.; Liu, S. Y. Fluorescent pH-Sensing Organic/Inorganic Hybrid Mesoporous Silica Nanoparticles with Tunable Redox-Responsive Release Capability. *Langmuir* **2010**, *26*, 15574−15579.
(35) Hu, X. L.; Liu, S. Y. Recent Advances Towards the Fabrication and Biomedical Applications of Responsive Polymeric Assemblies and Nanoparticle Hybrid Superstructures. *Dalton Trans.* **2015**, *44*, 3904−3922.
(36) Cho, D.-G.; Sessler, J. L. Modern Reaction-Based Indicator Systems. *Chem. Soc. Rev.* **2009**, *38*, 1647−1662.
(37) Basabe-Desmonts, L.; Reinhoudt, D. N.; Crego-Calama, M. Design of Fluorescent Materials for Chemical Sensing. *Chem. Soc. Rev.* **2007**, *36*, 993−1017.
(38) Germain, M. E.; Knapp, M. J. Optical Explosives Detection: from Color Changes to Fluorescence Turn-on. *Chem. Soc. Rev.* **2009**, *38*, 2543−2555.
(39) Chen, C. Y.; Chen, C. T. A PNIPAM-Based Fluorescent Nanothermometer with Ratiometric Readout. *Chem. Commun.* **2011**, *47*, 994−996.
(40) Hu, J. M.; Liu, S. Y. Responsive Polymers for Detection and Sensing Applications: Current Status and Future Developments. *Macromolecules* **2010**, *43*, 8315−8330.
(41) Hong, S. W.; Kim, D. Y.; Lee, J. U.; Jo, W. H. Synthesis of Polymeric Temperature Sensor Based on Photophysical Property of Fullerene and Thermal Sensitivity of Poly(N-isopropylacrylamide). *Macromolecules* **2009**, *42*, 2756−2761.
(42) Takei, Y.; Arai, S.; Murata, A.; Takabayashi, M.; Oyama, K.; Ishiwata, S.; Takeoka, S.; Suzuki, M. A Nanoparticle-Based Ratiometric and Self-Calibrated Fluorescent Thermometer for Single Living Cells. *ACS Nano* **2014**, *8*, 198−206.
(43) Adhikari, B.; Majumdar, S. Polymers in Sensor Applications. *Prog. Polym. Sci.* **2004**, *29*, 699−766.
(44) Allen, M. D.; Zhang, J. A tunable FRET Circuit for Engineering Fluorescent Biosensors. *Angew. Chem., Int. Ed.* **2008**, *47*, 500−502.
(45) Haustein, E.; Jahnz, M.; Schwille, P. Triple FRET: A Tool for Studying Long-Range Molecular Interactions. *ChemPhysChem* **2003**, *4*, 745−748.
(46) Tong, A. K.; Jockusch, S.; Li, Z. M.; Zhu, H. R.; Akins, D. L.; Turro, N. J.; Ju, J. Y. Triple Fluorescence Energy Transfer in Covalently Trichromophore-labeled DNA. *J. Am. Chem. Soc.* **2001**, *123*, 12923−12924.
(47) Bozdemir, O. A.; Erbas-Cakmak, S.; Ekiz, O. O.; Dana, A.; Akkaya, E. U. Towards Unimolecular Luminescent Solar Concentrators: Bodipy-Based Dendritic Energy-Transfer Cascade with Panchromatic Absorption and Monochromatized Emission. *Angew. Chem., Int. Ed.* **2011**, *50*, 10907−10912.
(48) Sun, Y. S.; Wallrabe, H.; Booker, C. F.; Day, R. N.; Periasamy, A. Three-Color Spectral FRET Microscopy Localizes Three Interacting Proteins in Living Cells. *Biophys. J.* **2010**, *99*, 1274−1283.
(49) Kawahara, S.; Uchimaru, T.; Murata, S. Sequential Multistep Energy Transfer: Enhancement of Efficiency of Long-Range Fluorescence Resonance Energy Transfer. *Chem. Commun.* **1999**, 563−564.
(50) Hannestad, J. K.; Sandin, P.; Albinsson, B. Self-Assembled DNA Photonic Wire for Long-Range Energy Transfer. *J. Am. Chem. Soc.* **2008**, *130*, 15889−15895.
(51) Liu, C. C.; Hang, H. Y. A progress in Detection of Interactions Between Macromolecules: Linked FRET Using Three Color Fluorophore. *Prog. Biochem. Biophys.* **2006**, *33*, 292−296.
(52) Heilemann, M.; Tinnefeld, P.; Mosteiro, G. S.; Garcia-Parajo, M.; Van Hulst, N. F.; Sauer, M. Multistep Energy Transfer in Single Molecular Photonic Wires. *J. Am. Chem. Soc.* **2004**, *126*, 6514−6515.
(53) Sapsford, K. E.; Berti, L.; Medintz, I. L. Materials for Fluorescence Resonance Energy Transfer Analysis: Beyond Traditional Donor-Acceptor Combinations. *Angew. Chem., Int. Ed.* **2006**, *45*, 4562−4588.
(54) Liu, J. W.; Lu, Y. FRET Study of a Trifluorophom-labeled DNAzyme. *J. Am. Chem. Soc.* **2002**, *124*, 15208−15216.
(55) Burghart, A.; Thoresen, L. H.; Chen, J.; Burgess, K.; Bergstrom, F.; Johansson, L. B. A. Energy Transfer Cassettes Based on BODIPY (R) Dyes. *Chem. Commun.* **2000**, 2203−2204.
(56) Serin, J. M.; Brousmiche, D. W.; Frechet, J. M. J. Cascade Energy Transfer in a Conformationally Mobile Multichromophoric Dendrimer. *Chem. Commun.* **2002**, 2605−2607.
(57) Watrob, H. M.; Pan, C. P.; Barkley, M. D. Two-step FRET as a Structural Tool. *J. Am. Chem. Soc.* **2003**, *125*, 7336−7343.
(58) Hu, X. L.; Hu, J. M.; Tian, J.; Ge, Z. S.; Zhang, G. Y.; Luo, K. F.; Liu, S. Y. Polyprodrug Amphiphiles: Hierarchical Assemblies for Shape-Regulated Cellular Internalization, Trafficking, and Drug Delivery. *J. Am. Chem. Soc.* **2013**, *135*, 17617−17629.
(59) Peggy, S.; Richard, S.; Patrick, S.; Yonetatsu, M. Polymerizable Copolymers for Alignment Layers [P] PCT: WO2005/014677.
(60) Hu, X. L.; Tian, J.; Liu, T.; Zhang, G. Y.; Liu, S. Y. Photo-Triggered Release of Caged Camptothecin Prodrugs from Dually Responsive Shell Cross-Linked Micelles. *Macromolecules* **2013**, *46*, 6243−6256.
(61) Yin, J.; Hu, H. B.; Wu, Y. H.; Liu, S. Y. Thermo-and Light-Regulated Fluorescence Resonance Energy Transfer Processes within Dually Responsive Microgels. *Polym. Chem.* **2011**, *2*, 363−371.
(62) Boyer, C.; Bulmus, V.; Davis, T. P.; Ladmiral, V.; Liu, J.; Perrier, S. Bioapplications of RAFT Polymerization. *Chem. Rev.* **2009**, *109*, 5402−5436.
(63) Boyer, C.; Stenzel, M. H.; Davis, T. P. Building Nanostructures Using RAFT Polymerization. *J. Polym. Sci., Part A: Polym. Chem.* **2011**, *49*, 551−595.
(64) Li, C. H.; Zhang, Y. X.; Hu, J. M.; Cheng, J. J.; Liu, S. Y. Reversible Three-State Switching of Multicolor Fluorescence Emission

DOI: 10.1021/acsami.5b04025
ACS Appl. Mater. Interfaces 2015, 7, 15551−15560

by Multiple Stimuli Modulated FRET Processes within Thermoresponsive Polymeric Micelles. *Angew. Chem., Int. Ed.* **2010**, *49*, 5120−5124.
(65) Li, C. H.; Hu, J. M.; Liu, S. Y. Engineering FRET Processes within Synthetic Polymers, Polymeric Assemblies and Nanoparticles via Modulating Spatial Distribution of Fluorescent Donors and Acceptors. *Soft Matter* **2012**, *8*, 7096−7102.
(66) Yu, Z.; Kabashima, T.; Tang, C.; Shibata, T.; Kitazato, K.; Kobayashi, N.; Lee, M. K.; Kai, M. Selective and Facile assay of Human Immunodeficiency Virus Protease Activity by a Novel Fluorogenic Reaction. *Anal. Biochem.* **2010**, *397*, 197−201.
(67) Hu, X. L.; Li, Y.; Liu, T.; Zhang, G. Y.; Liu, S. Y. Responsive Polymer-Based Multicolor Fluorescent Probes for Temperature and Zn2+ Ions in Aqueous Media. *Sci. China: Chem.* **2014**, *57*, 615−623.
(68) Demchenko, A. P.; Mély, Y.; Duportail, G.; Klymchenko, A. S. Monitoring Biophysical Properties of Lipid Membranes by Environment-Sensitive Fluorescent Probes. *Biophys. J.* **2009**, *96*, 3461−3470.
(69) Yu, Z.; Paul, R.; Bhattacharya, C.; Bozeman, T. C.; Rishel, M. J.; Hecht, S. M. Structural Features Facilitating Tumor Cell Targeting and Internalization by Bleomycin and Its Disaccharide. *Biochemistry* **2015**, *54*, 3100−3109.
(70) Liu, Y.; Joo, K. I.; Wang, P. Endocytic Processing of Adeno-Associated Virus Type 8 Vectors for Transduction of Target Cells. *Gene Ther.* **2013**, *20*, 308−317.
(71) Liu, T.; Hu, J. M.; Jin, Z. Y.; Jin, F.; Liu, S. Y. Two-Photon Ratiometric Fluorescent Mapping of Intracellular Transport Pathways of pH-Responsive Block Copolymer Micellar Nanocarriers. *Adv. Healthcare Mater.* **2013**, *2*, 1576−1581.

DOI: 10.1021/acsami.5b04025
ACS Appl. Mater. Interfaces 2015, 7, 15551−15560